Clinopyroxene megacrysts from Marion Island, Antarctic Ocean: evidence for a late stage shallow origin

R. James Roberts[1,*], Keabetswe D. Lehong[1], Andries E. J. Botha[1], Gelu Costin[2, 3],

Frikkie C. De Beer[4], Willem J. Hoffman[4] & Callum J. Hetherington[5]

[1]Department of Geology, University of Pretoria, Lynnwood Road, Pretoria, 0002, South Africa

[2]Department of Geology, Rhodes University, Artillery Road, Grahamstown, 6140, South Africa

[3]Department of Earth, Environmental and Planetary Sciences, Rice University, MS-126, 6100 Main Street, Houston, TX, 77005, USA

[4]Radiation Science Department, South African Nuclear Energy Corporation (Necsa), Elias Motsoaledi Street Extension (Church Street West), R104, Pelindaba, 0240, South Africa

[5]Department of Geosciences, Texas Tech University, Box 41053, Lubbock, TX, 79409-1053, USA

*Corresponding author: R. James Roberts. Email: james.roberts@up.ac.za

Abstract

Clinopyroxene megacrysts (up to 5 cm) from a scoria cone on Marion Island, Antarctic Ocean are zoned, with compositionally distinct low (Al + Ti) and high (Al + Ti) patches arranged haphazardly throughout crystals. Inclusions of olivine, pyrrhotite, oxides, sulphides, and rounded inclusions with euhedral micro-crystals interpreted as former melt inclusions are observed. Olivine inclusions have variable compositions, ranging from primary Ti-poor crystals to Ti-rich crystals hosting secondary haematite crystals formed by hydrogenation. The crystals contain voids that are concentrated in the middle of each crystal indicating that the initial crystal growth was skeletal. Subsequent crystallisation filled in the skeletal framework creating the patchy zoning in the crystals. The Marion Island megacrysts are not homogenous, but the combination of crustal clinopyroxene compositions, primary and hydrogenated olivine, and the mode of eruption in scoria eruptions indicates that these crystals most likely formed in a shallow magma chamber. Primary olivines crystallised from a mafic magma and secondary altered olivines were incorporated into a rapidly growing megacryst in a super-saturated, fluid-rich environment, prior to being ejected onto surface in a scoria eruption.

Keywords: Marion Island; Clinopyroxene megacrysts; Late stage eruption; Ankaramites

Introduction

Numerous locations across Marion Island in the sub-Antarctic Indian Ocean feature small deposits of megacrystic (>1 cm) clinopyroxene. These deposits have been described as scoria cones, and are considered to be a unique and separate volcanic

event in the chronology of Marion Island (Chevallier 1986). Megacrysts are commonly used as a tracer for magmatic evolution in the plumbing system of volcanoes, as crystals may feature zoning and growth patterns reflecting both long and short residence times in the ascending magma. Previous studies of Marion Island have focussed primarily on its structural evolution (Chevallier 1986), and volcanism and glaciation (Hall et al. 2011). Le Roex et al. (2012) described the petrology, mineral abundances and compositions, and bulk rock geochemistry of samples from Marion Island, and used the data to develop petrogenetic models for the compositional evolution of Marion Island lavas. According to Le Roex et al. (2012), the Marion Island lavas were formed by simple petrogenetic processes, of which the most notable features of the lavas are the uniform isotope and incompatible element ratios as well as the simplicity of the compositional variations (Le Roex et al. 2012). This study focuses on the clinopyroxene megacrysts from the island, which have not been described in detail, reports petrographic and geochemical analysis on the megacrysts, and suggests the mechanisms by which the crystals may have formed.

Geology of Marion Island

Marion Island (46 °54'S, 37 °45'E) is the younger of two volcanic islands known as the Prince Edward Island Group, situated in the sub-Antarctic Indian Ocean (Fig. 1). The Prince Edward Island Group is situated on the Antarctic Plate, 250 km south east of the South West Indian mid-oceanic ridge, striking 70 °. Marion Island forms the top part of an oval shaped shield volcano (Sumner et al. 2004; Chevallier 1986), and, together with the nearby Funk Seamount and neighbouring Prince Edward Island, may indicate the position of a "long lived" hotspot (McDougall et al. 2001). The surface topography of the island is dominated by scoria cones, pyroclastic flow deposits and exposures of younger black lava flows, with occasional exposures of older grey lavas (Chevallier 1986).

Marion Island is geologically young (<0.45 Ma) and its geology may be separated into three main units (Verwoerd 1971; Verwoerd et al. 1990). The older grey lava unit is between <450 ka and 100 ka in age, and consists of alkaline basalt lava flows interbedded with pyroclastics and intercalated tills from at least two eruptive periods, with the tills found at the beginning and the end of each of the volcanic periods (Boelhouwers et al. 2008). The younger black lava unit dates from ca. 11 ka to the present, with the last eruption in 1980. Scoria is present as a third unit throughout the island's history, and currently over 130 scoria cones are mapped in a semi radial pattern on the island (McDougall et al. 2001; Boelhouwers et al. 2008). Marion Island is regarded as an active volcano, as the last major eruption occurred in 1980 when a 9 km long en-echelon fissure opened on the western side of the island stretching from the coast to the summit. Petrologically, the black and grey lavas are predominantly alkaline basalts with SiO_2 values between 45 and 48 wt% (McDougall et al. 2001; Le Roex et al. 2012).

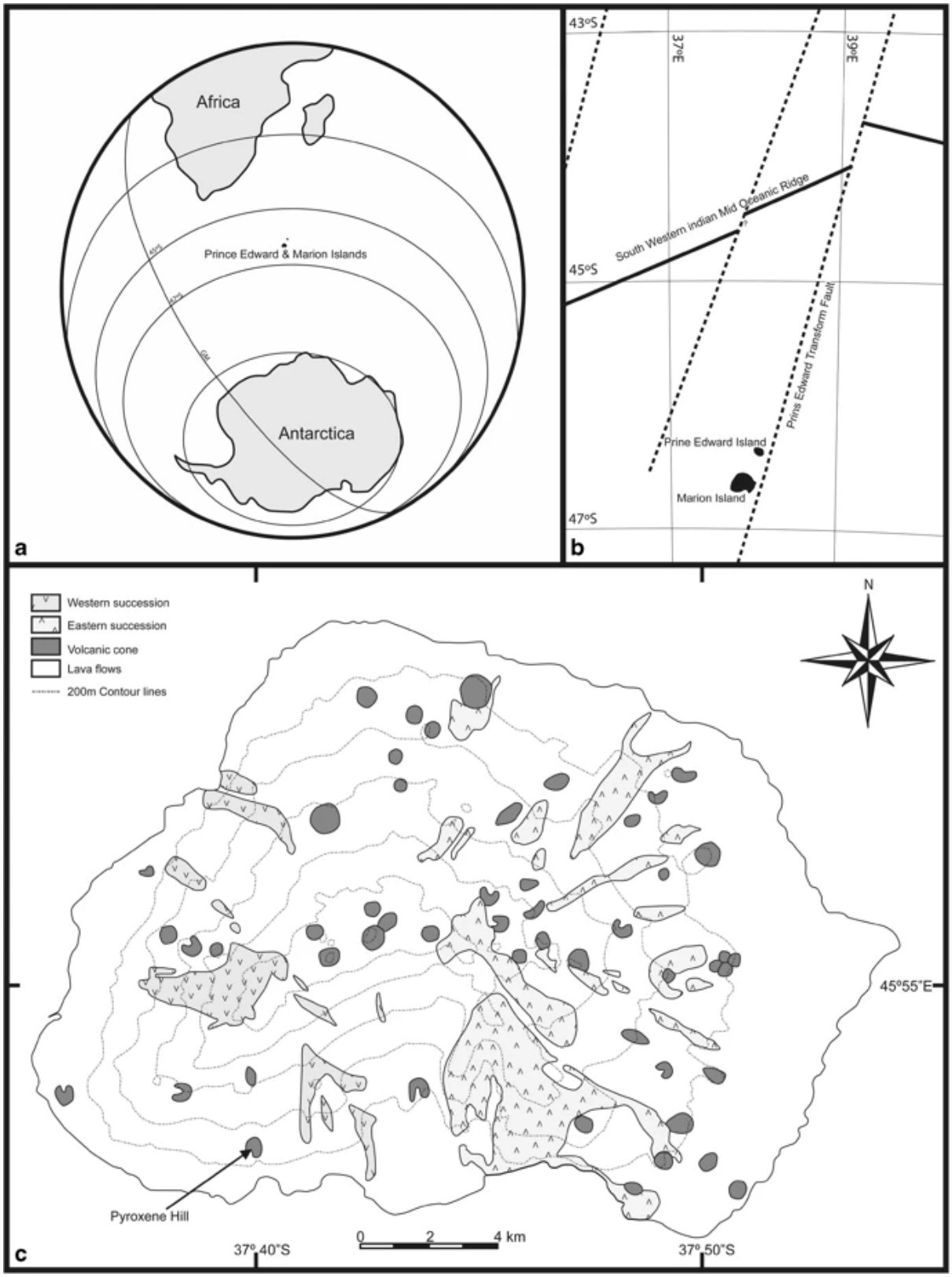

Fig. 1. The location of the Prince Edward Islands in the Southern Hemisphere (**a** and **b**), together with a simplified geological map of Marion Island (**c**), showing its volcanic and glacial evidence that assists in differentiating the two eruptive periods of the island (Holocene and Pleistocene). Arrow indicates sampling locality at Pyroxene Hill. Modified from McDougall et al. (2001)

Sampling and analytical methods

Sampling of Marion Island clinopyroxene crystals was done on the mid southern side of the island on a scoria cone named Pyroxene Hill (46 °56′36.29″S 37 °41′24.47″E; Fig. 1) in 2010. Three kg of crystals were sampled from the scoria cone, selecting the least weathered, most euhedral and coherent crystals. Crystal sizes vary between 3 mm and 5 cm.

The 225 kV micro-focus X-ray computed tomography (μXCT) system from Nikon Metrology was used to image the megacrysts, following Hoffman and De Beer (2012). Thirteen megacrysts were selected and arranged on the basis of sample diameter (smallest to largest). The X-ray source was operated at energies ranging between 60 and 100 keV and at currents of 80, 100, and 170 μA depending on the dimensions of the sample. A minimum of 1000 radiographs were collected for each sample in a 0–360 ° scanning interval with an acquisition time of about 30 minutes. Depending on the size of the sample, the spatial resolution achieved ranges from 7 to 20 μm. Additionally, Al (0.5 mm thick) was used as a filtering material to reduce X-ray beam hardening effects in the tomographic reconstruction. VGStudioMAX 2.2 analytical software package by Volume Graphics© was used for the visualisation and analysis of data derived from the μXCT system. This is inclusive of the construction of 3-D images and cross-sectional slices ("thin sections").

Imaging and analysis of selected crystals were conducted using the JSM-8500 LV scanning electron microscope (SEM) a Centaurus back-scattered electron (BSE) detector and a Thermo Scientific Noran System Seven (NSS) energy dispersive spectrometer (EDS). The Centaurus high-sensitivity BSE detector distinguishes between compositional domains where the difference in average atomic number (Z) is less than 1. Semi-quantitative mineral inclusion compositions were acquired using an accelerating voltage of 20 kV, with 1.1 s live time and 40 % dead time on the spectrometer. Additional BSE and micro-analysis was conducted on a Hitachi SN-4300 SEM. The instrument is equipped with a EDAX Pegasus 4040 EDS detector with EDAX Genesis software. Semi-quantitative micro-analysis was completed using a focussed and fixed electron-beam, an accelerating voltage of 15 kV, a detector dead-time of ~30 % and a ZAF-type matrix correction were applied during the data reduction process.

Electron-probe micro-analyzer (EPMA) analysis of clinopyroxene was done using a Cameca SX-100 at 20 kV and 20 nA, and 10 s counting time on peaks and 5 s for backgrounds on either side of the peak. Supplementary work on inclusions in the clinopyroxene was done on a JEOL JXA 8230 EPMA, using an electron-beam with a probe current of 20 nA, an accelerating voltage of 15 kV, and 10 s counting time on peaks and 5 s for backgrounds on either side of the peak. For each element analysed, reference materials used for the calibration of the characteristic Kα X-rays and average detection limits and average 1σ standard deviations are quoted in the following: Si (forsteritic olivine, 75 ppm, 0.22 %); Mg (forsteritic olivine, 76 ppm, 0.19 %); Fe (almandine, 315 ppm, 1.57 %); Al (almandine, 66 ppm, 45.9 %); Ca (Cr-diopside, 46 ppm, 5.2 %); Ti (rutile, 78 ppm, 80 %); Cr (chromite, 155 ppm, 250.9 % in olivine; 165 ppm and 1.2 % in clinopyroxene); Mn (rhodonite, 63 ppm, 6.9 %); Ni (pentlandite, 74 ppm, 4.22 %); Na (albite, 59 ppm, 0.94 %); K (orthoclase, 35 ppm,

15.5 %). Nickel, Ti, Mn and Ca were analyzed using large diffracting crystals with high sensitivity: LIFL for Ni and Mn, PETL for Ca and Ti. The ZAF matrix correction method was applied to data reduction and quantification.

Compositional maps of one crystal were collected using a Cameca factory SX--5 FE EPMA utilizing a field emission filament-gun operating with an accelerating voltage of 15 keV, and a probe-current of 60 nA. Mapped areas were collected in stage-map mode over an area of 2200 μm × 1000 μm, with a resolution of 1101 × 501 pixels (effective pixel size of 2 × 2 μm^2). A 40 ms dwell time per pixel and a stage scan of 2 μm step were used.

Trace element abundances in four crystals (2, 5, 6 and 10) were collected by laser-ablation inductively-coupled-plasma mass-spectrometry (LA-ICP-MS) using an Agilent 7500cs quadrupole mass spectrometer with a New Wave UP-213 solid state laser with dual-volume cell. Analytical spot-location was guided by large-area BSE-images collected by SEM, and the laser was operating using a frequency of 5 Hz, a spot size of 60 μm and a measured fluence of between 9 and 11 J/cm^{-2}. Data were reduced using the Excel-based GLITTER package using the NIST-610/612 glass to bracket every 8–10 analyses of pyroxene, Si abundances from micro-analyses were used as an internal standard, and USGS rock standard BHVO (Jochum et al. 2005) was used to monitor instrument performance, precision and accuracy.

Results: composition of clinopyroxene and its inclusions

Generalities

Petrography and compositional analyses show that the clinopyroxene megacrysts from Marion are not homogenous in composition. Petrographic observations reveal that olivine, sulphides, and spinel are present as inclusions within the megacrysts. The BSE images show the occurrence of an exsolved mineral phase in some olivine. Tomography and scanning electron imaging reveal that the clinopyroxene crystals are complex (Figs. 2 and 3), containing both empty space and inclusions. The empty space occurs as voids or pores within the crystals, concentrated at the centre of the crystals, and pseudo coloured in the μXCT images as dark (red) areas, representing no attenuation of the X-ray signal. The percentage of empty space (porosity) in the crystals can be calculated from the μXCT data (Table 1) and ranges from 1.69 vol% to 10.36 vol% for individual samples with analytic (statistical) error of ~ 5 % of the stated ranges.

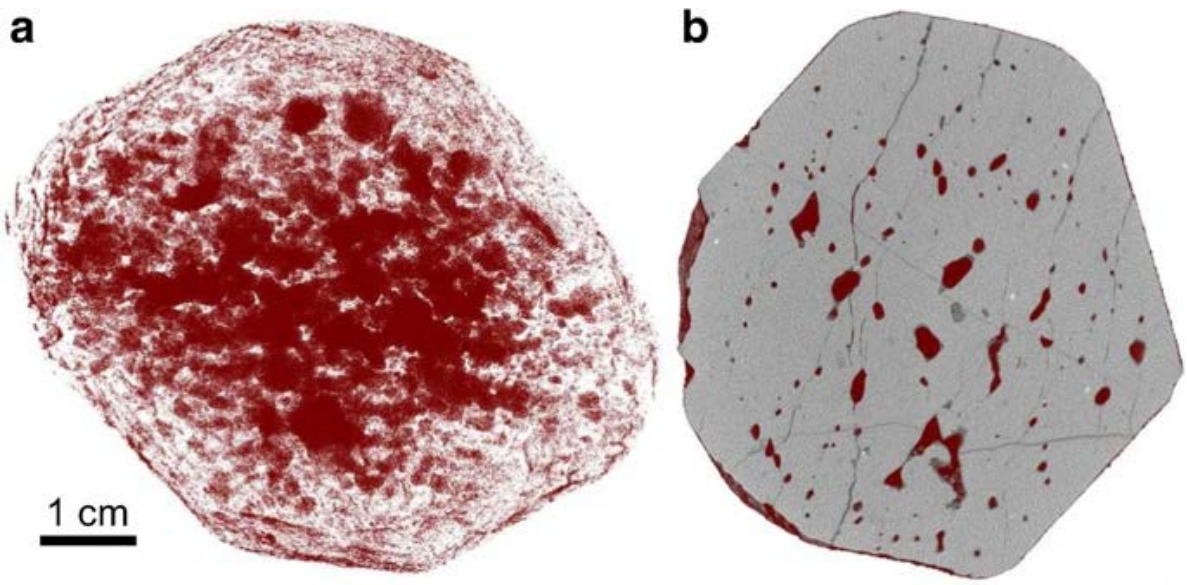

Fig. 2. μXCT slices showing the distribution of empty space within megacryst 6. **a** 3-Dimensional transparent image with pores (red) false coloured showing that most of the empty spaces occur at the centre of the megacrysts, and are interconnected with each other by fractures as seen in (**b**), a slice within the 3D-image

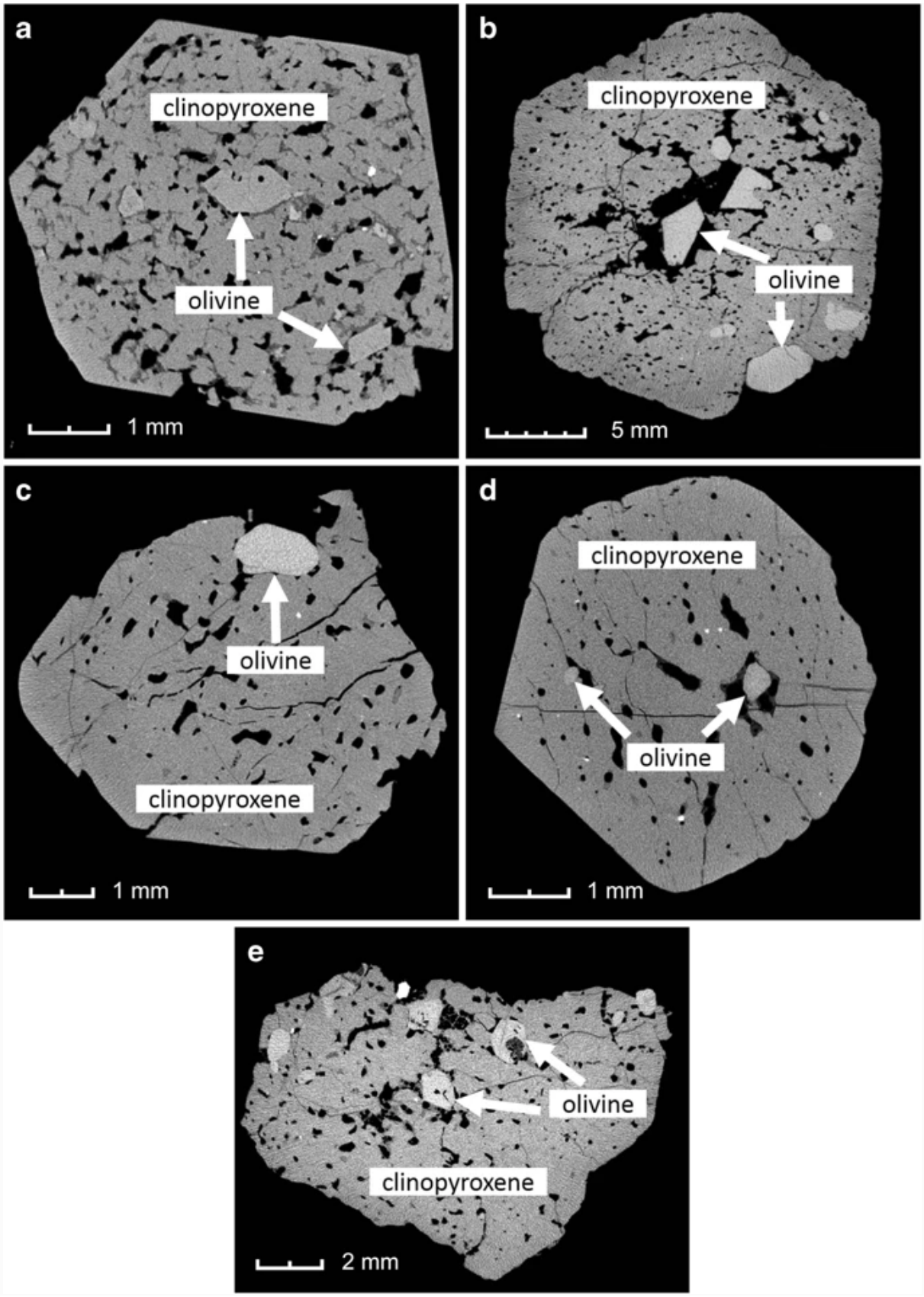

Fig. 3. Individual μXCT sample slices showing euhedral to subhedral crystals of olivine included within the clinopyroxenes megacrysts. **a** Numerous euhedral olivine inclusions (dark grey) in crystal 2; **b** euhedral and anhedral olivine inclusions (light grey) in crystal 4; **c** olivines showing haematite exsolution in crystal 5; **d** crystal 6; and **e** crystal 10

The inclusions occur in the core and in the rims of the crystals (Fig. 3), and include both euhedral and anhedral crystals. The rims of the crystals are relatively homogenous with fewer voids and inclusions than the cores of the crystals. Since the porosity is greatest towards the centre of the crystals, it is considered most likely that this porosity is primary in origin. If the porosity was secondary and caused by dissolution during later reaction with a fluid, porosity towards the rims would be expected.

Clinopyroxene

Back-scattered electron imaging, element distribution maps and spot-analysis reveal that the clinopyroxene megacrysts are diopside (Morimoto 1988) nd compositionally homogeneous with respect to Mg, Fe and Ca ($En_{42}Fs_{10}Wo_{48}$ to $En_{46}Fs_{08}Wo_{46}$). The abundances of Al_2O_3 vary between ~5 and 7.5 wt%, Na_2O is typically <0.5 wt%, and Cr_2O_3 is also present in abundances of <1 wt%. The calculated Ca/(Ca + Mg) × 100 and Mg/(Mg + Fe^{2+}) × 100 ratios are 52.5 and 79.7, respectively.

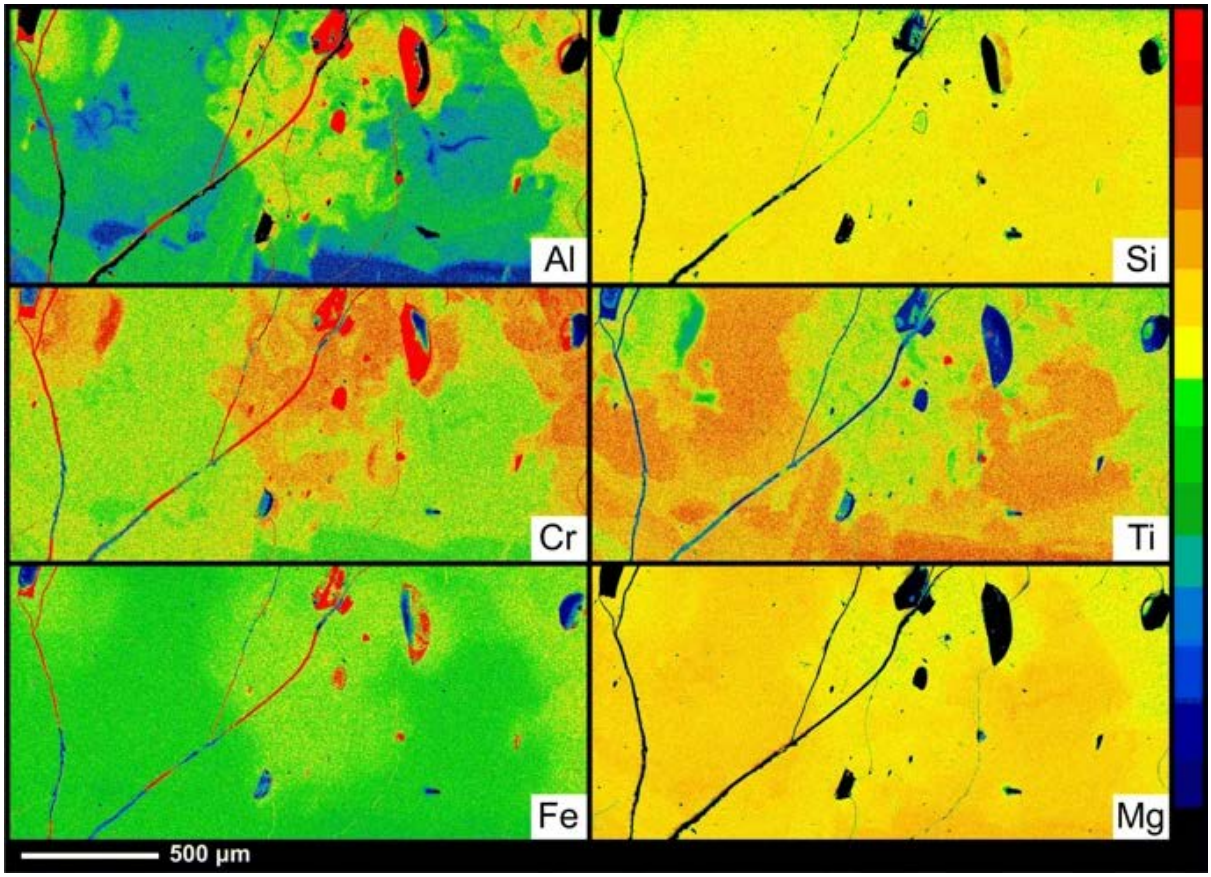

Fig. 4. Element maps of an area of 2200 µm × 1000 µm, colour coded to the counts measured by FE-EPMA. The patchy nature of the crystals is clearly visible, showing low Al-Ti and high Al-Ti clinopyroxene patches. The borders between the different patches vary from sharp to diffuse, reflecting the difference in diffusion rates between different crystals. Colour bar is scaled to the counts recorded for each element: Al (212–422 cts), Si (544–1400 cts), Cr (0–100 cts), Ti (0–75 cts), Fe (0–120 cts) and Mg (385–1125 cts)

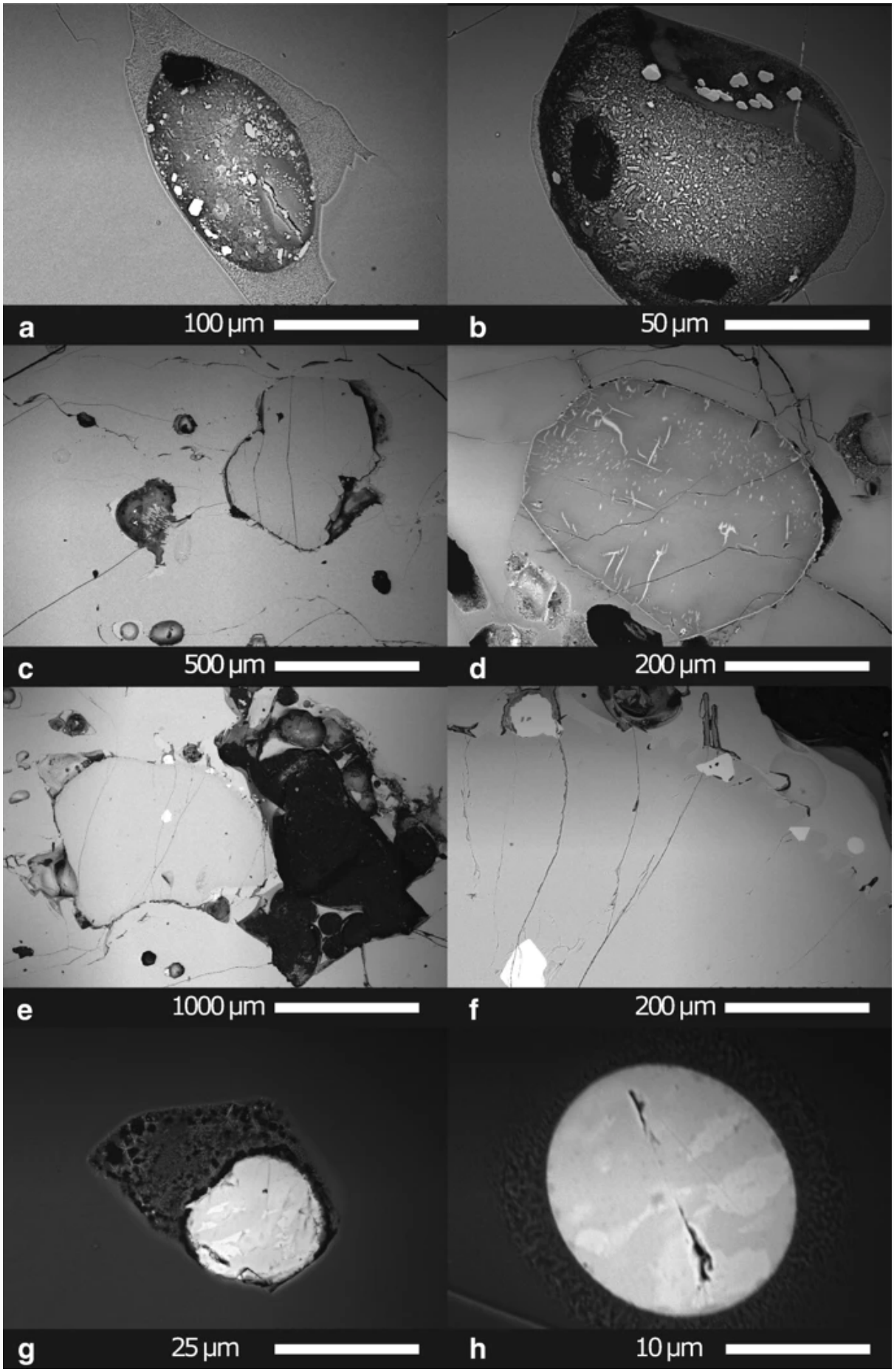
a
100 µm
b
50 µm
c
500 µm
d
200 µm
e
1000 µm
f
200 µm
g
25 µm
h
10 µm

Fig. 5. Back-scatter electron images of inclusion phases and textures in clinopyroxene (Cpx) megacrysts. **a**, **b** Glass melt inclusions that have crystallised a variety of high BSE intensity euhedral inclusions, the majority of which are Fe-oxide phases. **c** Image of an olivine (Ol) and a melt inclusion in the clinopyroxene. Note the dark rim around the olivine demonstrating the absence of a crystallographic relationship between the inclusion and the host clinopyroxene. **d** An altered olivine inclusion with streak-like to small elongate inclusion of an Fe-oxide phase surrounded by halos of BSE-darker, Mg-richer olivine. **e** Olivine inclusion with high-BSE intensity phases occuring as inclusions or along grain boundaries between olivine and clinopyroxene. **f** Higher-magnification image of the olivine grain boundary (see part **e**) with spinel (Spl), Fe-Cu-oxide, pyrite (Py) and Fe-Cu-Ni-sulphide inclusions near olivine rim. Note the slightly darker BSE intensity dentate grain boundary of olivine. **g**, **h** Pyrite (FeS) with complex intergrowths of Fe-Ni- and Fe-Cu-sulphide phases such as pentlandite (Pn) and chalcophyrite (Ccp)

The compositional data and imaging (Fig. 4; Table S1 in the Electronic Supplementary Material) show two compositional domains, each with a discrete range of elements, enabling a subdivision into low-Al-Ti and high-Al-Ti clinopyroxene. The majority of the clinopyroxene is low-Al-Ti, which hosts irregular patches of high-Al-Ti. The boundaries between the regions range from sharp to gradational. The low-Al-Ti patches have higher Mg and Cr abundances.

Melt inclusions within clinopyroxene

The BSE images of the clinopyroxene megacrysts show the presence of a significant number and type of inclusions. The most numerous population of inclusions are interpreted to represent entrapped droplets of melt (Fig. 5a–c). They are typically between 75 and 150 μm in size and have a rounded to slightly elongate shape. These inclusions are rarely in direct contact with the pyroxene host, having a fine-grained matrix between them and the host pyroxene. They have complex textures, and are compositionally similar to the pyroxene host (Fig. 5a). The inclusions are not a homogenous phase and themselves have crystallised numerous inclusions, the majority of which have euhedral to subhedral form, and have a high BSE intensity (Fig. 5a, b). The EDS analyses show that the high BSE-intensity crystals in the melt inclusions are an Fe-oxide phase. An integrated EDS analysis of whole melt-inclusions indicates that they have a range of compositions, but are generally mafic (~50 wt% SiO_2), contain appreciable ($Na_2O + K_2O$) (~5 wt%) and TiO_2 (2–3 wt%), alongside Al_2O_3, MgO and CaO abundances of ~12.5 %, 6–8 wt% and 8–10 wt% respectively, and FeO contents of 9–15 wt%.

Olivine

Olivine inclusions constitute about 5 % of most clinopyroxene megacrysts and are found within the main mass of the crystals and on the edges of pores (Fig. 5; Table S2 in the Electronic Supplementary Material). Olivine predominantly occurs as an aggregate of grains that are sub- to anhedral, with conchoidal fractures that do not cross grain boundaries (e.g. Fig. 3). The olivine grains vary in size from 200 to ~600 μm and are identifiable in BSE images and element maps (Fig. 5; Table S2 in the Electronic Supplementary Material). The olivine inclusions are forsteritic (Fo79 to Fo90) and may contain up to 0.8 wt% TiO_2, 0.18 wt% CaO, and 0.29 wt% Al. The inclusions are surrounded by a thin amorphous rim indicating that there is no crystallographic relationship between the olivine and its host pyroxene.

A sub-set of the olivine inclusions, based on BSE intensities, display complex internal textural zoning (Fig. 5d). Around the rims and in select areas in their interior, grains have a weak BSE intensity. Along the rim of these grains, and in the middle of the darkest BSE intensity domains, are high BSE intensity domains. There is an intermediate BSE intensity phase that reflects the composition of primary olivine with no alteration textures. The brightest BSE zones, which occur as streak-like structures or small (<10 μm) slightly elongate inclusions have no distinct grain boundaries with their host, and are very Fe-rich. The thin (<1 μm) rims around the edge of the olivine grain are similarly Fe-enriched. The darker BSE halos around the Fe-rich, high-BSE intensity zones are more Mg-rich in composition compared to the primary olivine.

Olivine grains themselves contain high BSE intensity inclusions, which, based on the absence of alteration halos in the host olivine or a well-defined grain boundary, are proposed to be primary (Fig. 5e). Similar inclusions are occasionally found in the clinopyroxene, or, as phases along the boundaries between the olivine and pyroxene host (Fig. 5f). The boundary of the olivine has a dentate texture, and the margin of the olivine has a slightly darker BSE intensity. These bright BSE intensity phases were identified, using EDS-based compositional analysis, as an Al-Mg-Cr-Fe-oxide phase with minor Ti, probably of the spinel family, pyrrhotite ($Fe_{(1-x)}S$), cupro-spinel, a Fe-Cu-oxide phase that may be an intermediate solid-solution between magnetite and cuprospinel, and, a complex intergrown Fe-Ni-Cu-sulphide phase that is dominated by pyrrhotite, but may also contains pentlandite and chalcopyrite (Fig. 5g, h; Tables S3 and S4 in the Electronic Supplementary Material). These Fe-Ni-Cu-sulphide inclusions are commonly rounded and may represent immiscible melt droplets.

Trace element profiles in clinopyroxene

Based on the decreasing abundance of inclusions and pores from core to rim, and their near absence in the euhedral rim, analytical spots for LA-ICP-MS were located in transects from rim-to-core-to-rim of each crystal, as well as around the rims of each crystal (Table S5 in the Electronic Supplementary Material). The LA-ICP-MS data for Ti and Al reflect the correlation observed in the EPMA data, and the increasing Ti and Al abundances positively correlate with V, Mn (Fig. 6) and Zr, and negatively with Cr and Ni. Chondrite normalized REE patterns show a humped pattern with a positive slope between La and Sm, and a negative pattern between Sm and Lu, which has constant slope (Fig. 7). The chondrite normalized REE patterns show no systematic pattern or positive or negative anomalies, and no relative enrichment or depletion as a function of the location of the analysis point relative to core and rim. However, there is a positive correlation between the measured abundance of ΣREE with increasing Al and Ti.

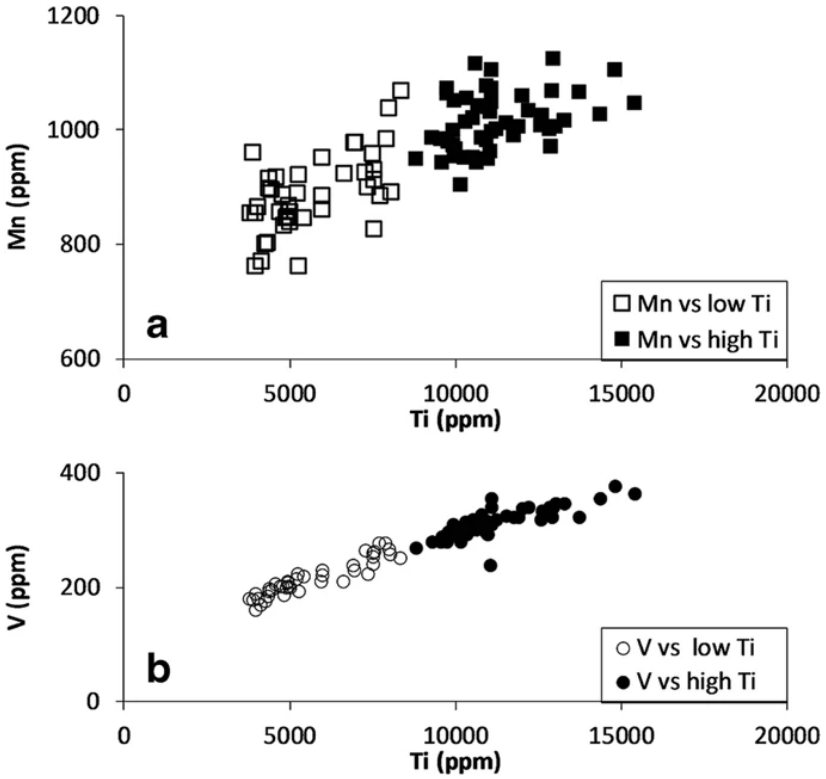

Fig. 6. Trace element abundances from LA-ICP-MS analysis of the crystals. **a**, plot of Mn against Ti; **b**, plot of V against Ti. Both Mn and V increase with increasing Ti. Open symbols represent low-Al-Ti patches and filled symbols represent high-Al-Ti patches. A complete continuum can be seen in the diagram

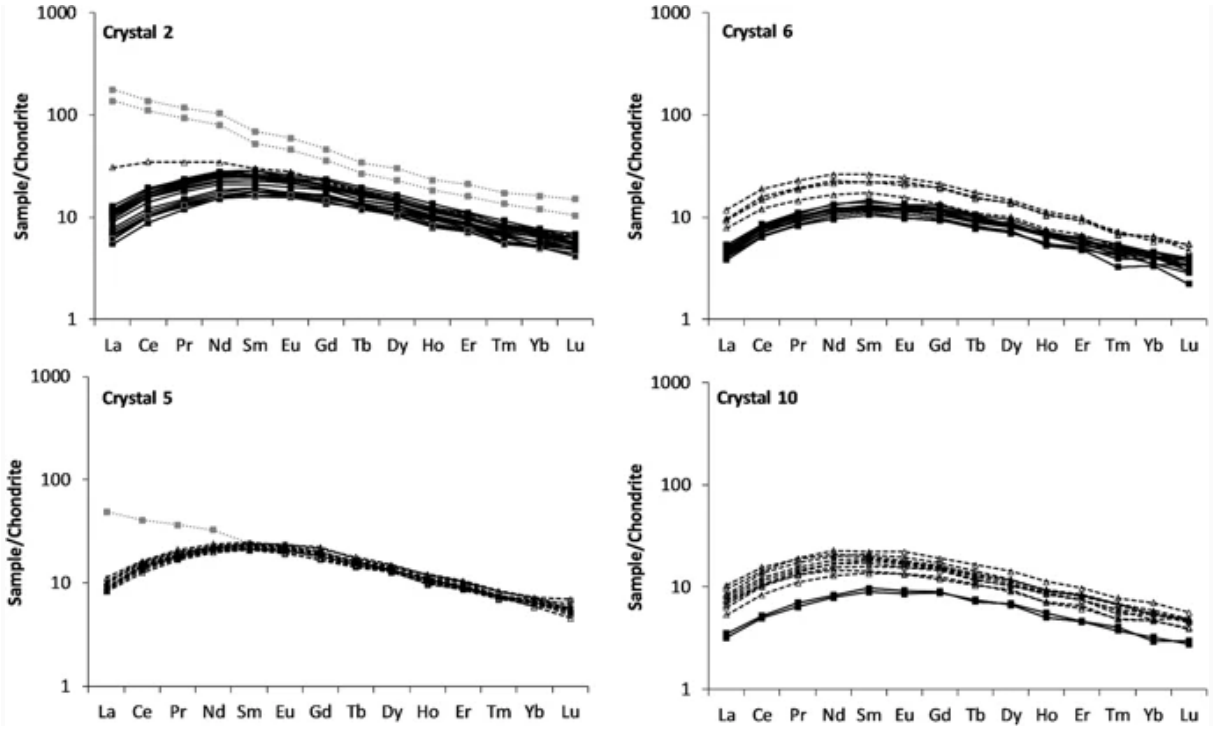

Fig. 7. Chondrite normalised REE profiles from analysed Marion clinopyroxene crystals analysed by LA-ICP-MS. Black profiles are from low-Al-Ti patches, dotted black lines are from high-Al-Ti patches Light grey dotted profiles are taken from the rims of the crystals. Chrondite normalisation values are from Sun and McDonough (1989)

Discussion

The origin of olivine within the clinopyroxene megacrysts

Olivine is the most common mineral inclusion in the clinopyroxene megacrysts, and has Fe-mole ratios between 0.10 and 0.21. The olivine inclusions are also characterised by low concentrations of Cr_2O_3 (0 to 0.04), and NiO concentrations between 0.11 and 0.27 wt%. The depletion of Fe in the olivine halo surrounding the Fe-rich inclusions suggests an alteration process that partitioned Fe into the high-BSE-intensity phase. Based on EDS compositional analyses, the high BSE-intensity phase is a Fe-oxide (haematite or magnetite). There is no internal grain boundary between primary and secondary olivine, and coupled with the compositional changes, it is proposed that the alteration may have proceeded via a dissolution-reprecipitation process, which is known to be fluid-aided (Putnis 2002). The compositional range observed, as well as the presence of primary and altered olivines, suggest that the Marion Island olivine inclusions are sourced at different depths.

By integrating the μXCT and imaging data, it is observed that in crystals with low porosity, (e.g. crystals 2 and 10) the majority of the olivines are unaltered (Fig. 3a). In contrast, in crystals with greater porosity (e.g. crystals 4 and 5), unaltered olivines are predominantly found towards pyroxene cores (Fig. 3b), and altered olivines are more common towards pyroxene rims. This relationship implies that altered olivines were either incorporated into the outer layers of the clinopyroxene during their growth, or fluid infiltration was limited to the outermost zones of the megacrysts. As the outer layers are relatively low in porosity in most crystals, it is considered likely that the olivines were already altered prior to incorporation. There is no systematic relationship between the olivines and the clinopyroxene domains, which further supports the idea that already altered olivines were incorporated into the growing clinopyroxene.

In the Marion olivine, TiO_2 abundances are as high as 0.81 wt%, and several populations of olivine based on TiO_2 content may be distinguished (Fig. 8). The compositions of the olivines are indicative of olivines formed at crustal depths, as the unaltered olivines are between Fo79 and Fo83, and have low Cr and Ni and high Ca, Ti and Al. The textural relationship between the olivines and the host clinopyroxenes indicates that the olivines were incorporated into the megacrysts within the magmatic plumbing system, rather than being transported from depth. The presence of a Fe-rich oxide within the some of the olivines merits further consideration.

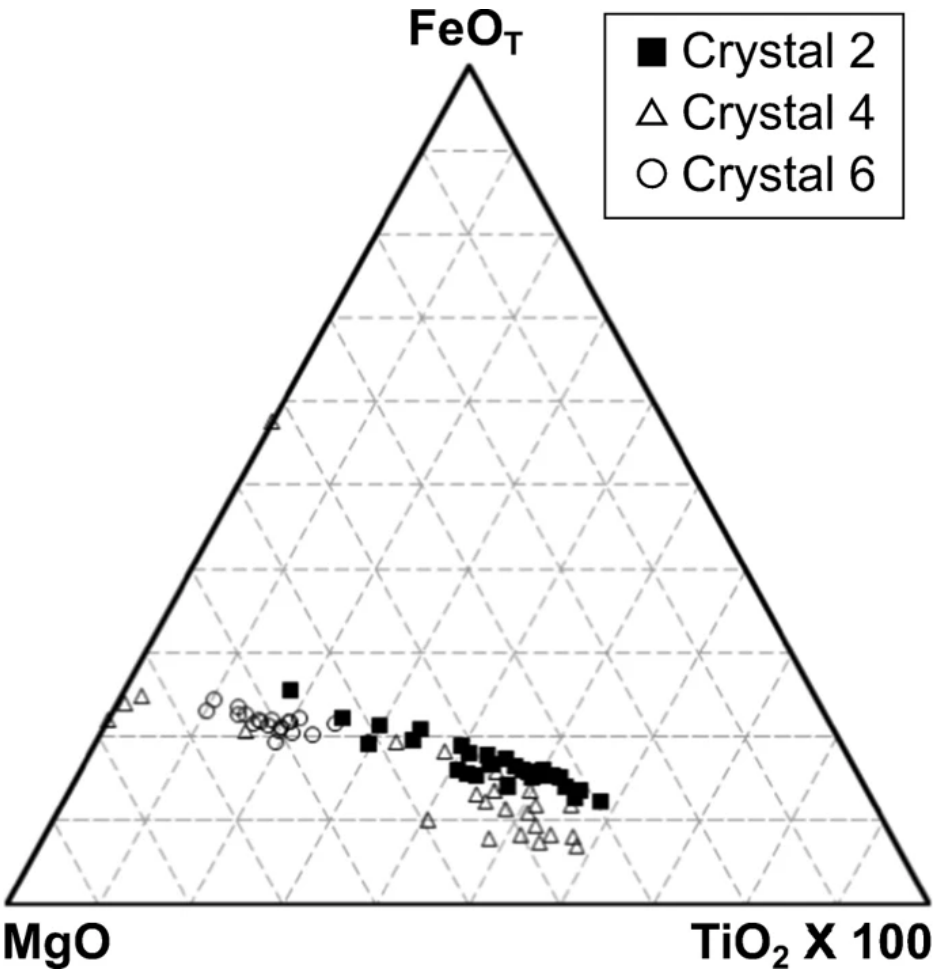

Fig. 8. MgO-FeO_T-TiO_2 × 100 ternary diagram showing the composition of olivine changing from a constant initial Mg:Fe ratio to more enriched in Mg. FeO_T (FeO_{total}) is used as all Fe in olivine is assumed to be in 2+ oxidation state. The olivines from three different crystals are shown, indicating that the olivine population is not homogenous across the whole megacryst population. TiO_2 concentrations also vary significantly for the olivine inclusions, suggesting that some olivines have been altered

Several studies have reported haematite precipitates in mantle olivines, that grew by processes that may be relevant here. The oxidation of mantle olivine commonly produces haematite precipitates within the interior of olivine (Champness 1970) and is consistent with the documented increase in Mg# for olivine inclusions with haematite found in the Marion Island pyroxene megacrysts. The occurrence of haematite precipitates has also been reported in lab experiments and in other natural samples where oxidisation of olivine occurred at high temperatures (Champness 1970; Kohlstedt and Vander Sande 1975). The recurring appearance of haematite lamellae in the olivine inclusions of Marion Island megacrysts suggests that oxidation-induced haematite was an important process contributing to the textural complexity of the assemblage (Hwang et al. 2008). Because not all olivine inclusions display the texture the processes occurred prior to incorporation in the clinopyroxene megacrysts.

Haematite has been proposed to form in mantle olivine via the following chemical reaction (Kohlstedt and Vander Sande 1975):

$$2Fe_2SiO_4\ (\text{olivine}) + O_2 \rightarrow 2Fe^2O_3\ (\text{haematite}) + 2SiO_2 \quad (1)$$

However, no evidence of a silica phase is observed in the Marion olivines, so different oxidation scenarios must be considered (Khisina and Wirth 2002; Dyar et al. 1998; Ingrin and Skogby 2000). The most convincing alternative requires that the exhumation history of the crystals be taken into account (Hwang et al. 2008). Olivine formed lower in the Marion plumbing system is transported by magma to shallower depths in the Earth's crust where temperatures are between 550 °C and 650 °C. Hydrogen may be incorporated in the crystal lattice of olivine during magma ascent to shallower depths, especially if the transporting magma is water-bearing. Hydrogen diffusion results in the oxidation of Fe^{2+} to Fe^{3+}, which causes the precipitation of haematite along the weak cleavage planes or dislocations in olivine (Hwang et al. 2008). This process is referred to as dehydrogenation-oxidation (Ingrin and Skogby 2000), and causes haematite precipitation via the following reactions:

$$2Fe^{2+} + OH \rightarrow 2Fe^{3+} + 2O^{2-} + H_2 \quad (2)$$

$$2Fe^{2+} + 2H^{+} \rightarrow 2Fe^{3+} + H_2 \quad (3)$$

Fe^{3+} is released from the olivine crystal lattice resulting in haematite precipitating in olivine at shallower depths via the following reaction:

$$x(FeMg)_2SiO_4 + 3O \rightarrow Fe_2O_3 + yMg_2SiO_4 \quad (4)$$

Dehydrogenation is accompanied by the generation of secondary metamorphic olivine (Jan et al. 2014). For the Marion Island olivine, the fractured nature of the inclusions together with the occurrence of magnetite supports a model where some olivine, or domains in olivine, are secondary. Secondary metamorphic olivine is marked by high TiO_2 contents (up to 0.85 wt.%), correlating with H_2O of up to 0.7 wt.% in the system (Jan et al. 2014). Similarly, De Hoog et al. (2014) reported that primary olivine in mafic magmas is Ti-poor (0–0.025 wt.%) and second generation metamorphic olivine is Ti-rich with TiO_2 content of up to 0.85 wt.%. The Marion olivines (Fig. 8) show a range in TiO_2 that extends from 0.2 to 0.8, so it possible that the olivine inclusions represent both primary, early crystallised olivine as well as altered olivine produced at shallow depths in a water-rich environment. However, none of the olivines are particularly Ti-poor, and a mantle origin is not indicated for any grains.

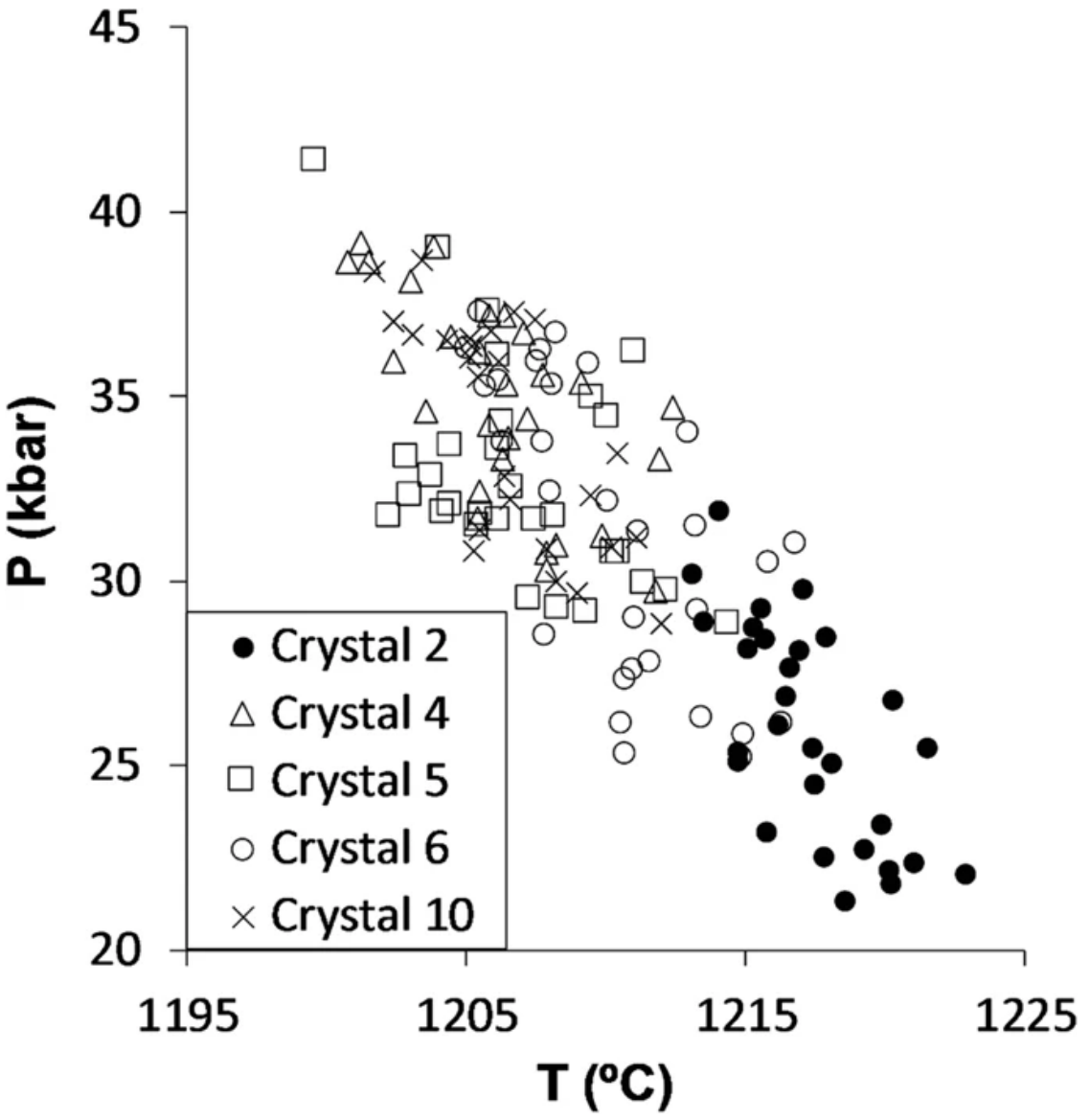

Fig. 9. Single clinopyroxene geobarometry and geothermometry (Putirka 2008, modified from Nimis and Taylor 2000). It can be seen that the calculated depths of formation based on Cr and Al cover a wide range, whereas temperatures, based on Na and K, are constrained to a relatively narrow range

Clinopyroxene barometry

To determine the pressures under which the clinopyroxene megacrysts and their associated inclusions may have crystallised, a single clinopyroxene geobarometer based on the partitioning of Cr and Al in the clinopyroxene lattice was applied (Nimis and Taylor 2000). The original equations have been recalibrated by Putirka (2008; eq. 32a), and provide one possible method of determining the depth of formation for the Marion Island crystals. The barometry (Fig. 9) produced a possible crystallisation pressure range of between 20 and 45 Kbar (55–90 km depth at 3.7 km per 0.1 GPa; Spear 1993). Liquidus temperatures between 1200 °C and 1220 °C are also calculated from the partitioning of Na and K in clinopyroxene (eq. 32d in Putirka (2008)). The modelled pressures vary greatly between crystals, whereas temperature is relatively well-constrained. Crystal 2 is calculated to crystallise between 20 and 30 kbar, whereas crystals 4, 5 and 10 crystallised between 30 and 40 kbar, and crystal 6

crystallised over the entire pressure range. The calculated relationship between T and P is also problematic, as lower temperatures are calculated for deeper depths. This may reflect a problem with the partitioning of Cr and Al (pressure) in the Marion crystals, relative to the partitioning of Na and K (temperature).

Hammer et al. (2016) described clinopyroxene megacrysts from the Haleakala ankaramite, and highlighted a number of problems with using such barometric methods on crystals such as those from Marion Island. The underlying assumption behind all thermobarometric modelling is that the crystals were in equilibrium with the host liquid. The presence of primary and altered olivine inclusions in the clinopyroxenes shows that the crystals have formed over a range of oxygen fugacities, which indicates that the host liquid was evolving in composition as the clinopyroxene crystals grew. Mollo et al. (2013) noted that rapid growth inhibits ideal partitioning of trace elements further complicating the application of thermobarometry on large crystals. Hammer et al. (2016) concluded that the barometry on the Haleakala clinopyroxenes significantly over-estimated the temperature and pressure of formation, as the partitioning of elements into the clinopyroxene was not temperature and pressure dependent, but rather controlled by kinematic constraints related to the speed of crystal growth. A similar conclusion likely applies to the Marion Island clinopyroxenes, which display patchy zoning and great size.

Zoning of the clinopyroxenes

The most unusual feature of the Marion Island clinopyroxene megacrysts is the subtle but pervasive patchy zoning found through the crystals. Patchy zoning in magmatic crystals, first defined by Vance (1965), involves an intricate, complex arrangement of zones of different composition within the crystal (Streck 2008). Patchy zoning is suggested to have formed in one of two ways: crystals undergo incomplete diffusion during the process of re-equilibration; or, evolved melt crystallises in the cavities of an early-formed skeletal crystal, in which case the younger crystallisation has a different composition (Streck 2008). Distinguishing between patchy zoning caused by diffusional re-equilibration versus crystal growth may be done on the basis of the sharpness of compositional change between different patches. According to Stewart and Pearce (2004), a sharp or step-like change between neighbouring patches is indicative of crystal growth, whereas Tomiya and Takahashi (2005) demonstrated that gradual compositional change between neighbouring domains is indicative of diffusional re-equilibration.

The Marion Island samples closely match the physical parameters for an early formed skeletal crystal with later in-filling of the cavities because the compositional boundaries between domains are either sharp, or show step-like sharp boundaries on the element maps and BSE images (Fig. 4). However, the presence of more gradual boundaries could also indicate that diffusion processes may have occurred between two contrasting domains in some crystals (Figs. 4 and 5). It is thus possible that the zoning is created by a mixture of processes, rather than a single dominant process.

Clinopyroxene composition is controlled by the partitioning of different elements into the two octahedral sites in the structure. These M-sites in the clinopyroxene structure will accommodate trace elements, but the M2 site, being slightly larger, will preferentially partition ions of larger ionic radius, including Sr^{2+} and the REE^{3+}, and

likely participate in a coupled substitution with Na^{+} or comparable lower charge, smaller ions. In contrast, the smaller 1st row transition series elements including Sc, V, Ni and Cr are more preferentially accommodated in the M1 site, presumably participating in a substitution with Mg^{2+} and Fe^{2+}.

The textural relationships between the high and low Al domains suggest that the lower Al-Ti compositions represent early crystal growth, with the higher-Al-Ti zones being younger. Both low and high Al-Ti domains are higher in Al, Ti and Fe^{3+} than would be expected in a primitive basaltic magma, and are both higher in Al and Ti than the clinopyroxenes in the lavas that comprise the bulk of Marion Island (Le Roex et al. 2012). Loucks (1990) suggested that the incorporation of Al and Ti into clinopyroxene is controlled by two charge-coupled substitutions: 1) the $^{vi}Mg^{iv}Si_2 \leftarrow\rightarrow\rightarrow\leftarrow {}^{vi}Ti^{iv}Al_2$ substitution, which is controlled by Ti activity within the melt, and 2) the $^{vi}Mg^{iv}Si \leftarrow\rightarrow\rightarrow\leftarrow {}^{vi}Fe^{3+}\,{}^{iv}Al$ substitution, which is controlled by H_2O and O_2 fugacity in the melt. Both substitutions would be favoured in a shallow, late-stage and low volume magma with high water content, a conclusion supported by the presence of inclusions of secondary olivine.
The abundance of empty space ("porosity") within the core of the crystals may also indicate that the earliest crystal growth was skeletal, as these voids are concentrated in the centre of each crystal and are not necessarily connected to the surface of the crystal. These voids are problematic, as there is no evidence that these voids were ever filled with either glass ("melt") or another crystalline phase that has since been dissolved out. A radical suggestion would be that the voids in the initial skeletal framework were gas-filled and sealed-in by later extremely rapid crystallisation.

A model for the Marion Island megacrysts

Textural and compositional data collected from the megacrysts are somewhat contradictory. The thermobarometry suggests a mantle origin for the megacrysts, but the calculated depths are questionable because such large crystals, particularly with patchy zoning, may not have grown in compositional equilibrium with their parental magma. In addition, the composition of the crystals does not reflect that of peridotitic clinopyroxene. At the same time, olivine included in the clinopyroxenes is relatively Ti-rich, indicative of crystallisation from an evolved magma. Haematite exsolution in some of the olivines may indicate rapid ascent and hydrogenation at shallow crustal depths and low temperatures. Thus, the megacrysts appear to have both mantle and crustal components.

Supersaturation is required for the growth of such large crystals, implying that the crystals must have grown at non-liquidus temperatures. An initial skeletal phase has been followed by in-fill crystallisation, and finally by the crystallisation of a euhedral rim. A similar situation was posited on ankaramitic clinopyroxenes from Halaekala on Hawaii (Welsch et al. 2016; Hammer et al. 2016).

In the Marion Island case there is evidence that water was involved in the growth of the megacrystals. The host scoria cones are found throughout the geological history of the island, and several have erupted during human history (Chevallier 1986). Super-saturation in a basaltic melt is rare, but may occur through the advent of second boiling, releasing volatiles during pressure driven ascent and dropping the liquidus temperature for phases such as clinopyroxene. Such second boiling is a

near-surface phenomenon that occurs in the final stages of magma chamber crystallisation. Mollo and Hammer (2017) reported the results of several experimental studies on clinopyroxene, and noted that rapid decompression favours the production of clinopyroxene over plagioclase, an effect that can be enhanced by multiple decompression episodes.

If this model is correct, the Marion Island megacrysts represent the final stages of crystallisation of a magma chamber, when crystallisation has reduced the temperature and evolved the composition of the magma to a point where volatiles are no longer soluble in the siliceous magma. Alternatively, surface water could percolate down into the magma chamber to drive supersaturation. In either process, the clinopyroxene megacrysts are essentially a late-stage near-surface manifestation of crystallisation processes. The olivine inclusions thus represent both peritectic crystals entrained by ascending magma, and metamorphic olivine produced in the magma chamber or on the walls of the conduit. The olivine and clinopyroxene do not share a common magmatic history, and the clinopyroxenes themselves are most likely formed in a shallow magmatic plumbing system hosted within the crust below the Marion volcanic edifice.

Though the Marion Island megacrysts are not ankaramites in the strict sense defined in Le Maitre et al. (2005), as they are not associated with plagioclase or basanitic magmas, their appearance and size is similar to the ankaramites reported on many ocean islands. In Fig. 10a, it can be seen that the compositions of the Marion megacrysts have higher Al/Ti and lower Mg/Fe ratios than the clinopyroxene crystals found in the volcanic rocks on Marion (data from Le Roex et al. 2012). However, there is a linear trend from the volcanic crystals to the megacrysts, which may indicate a genetic link. Similar linear relationships exist between the Haleakala ankaramitic clinopyroxenes and their host lavas, and between the Jan Mayen ankaramatic clinopyroxenes and their host lavas (Fig. 10b). Hammer et al. (2016) and Welsch et al. (2016) have reported large skeletal clinopyroxene crystals with patchy zonation from Haleakala as well. Thus, there is evidence that the same evolving magma produces both the voluminous basaltic lavas on Marion and the megacrysts, and similar processes may be responsible for the production of ankaramites on other ocean islands, i.e. ankaramitic clinopyroxenes are process-related and not related to a particular magma composition. More work needs to be done on the ankaramitic clinopyroxenes from other ocean islands to see if these crystals have characteristics similar to those of the Marion megacrysts.

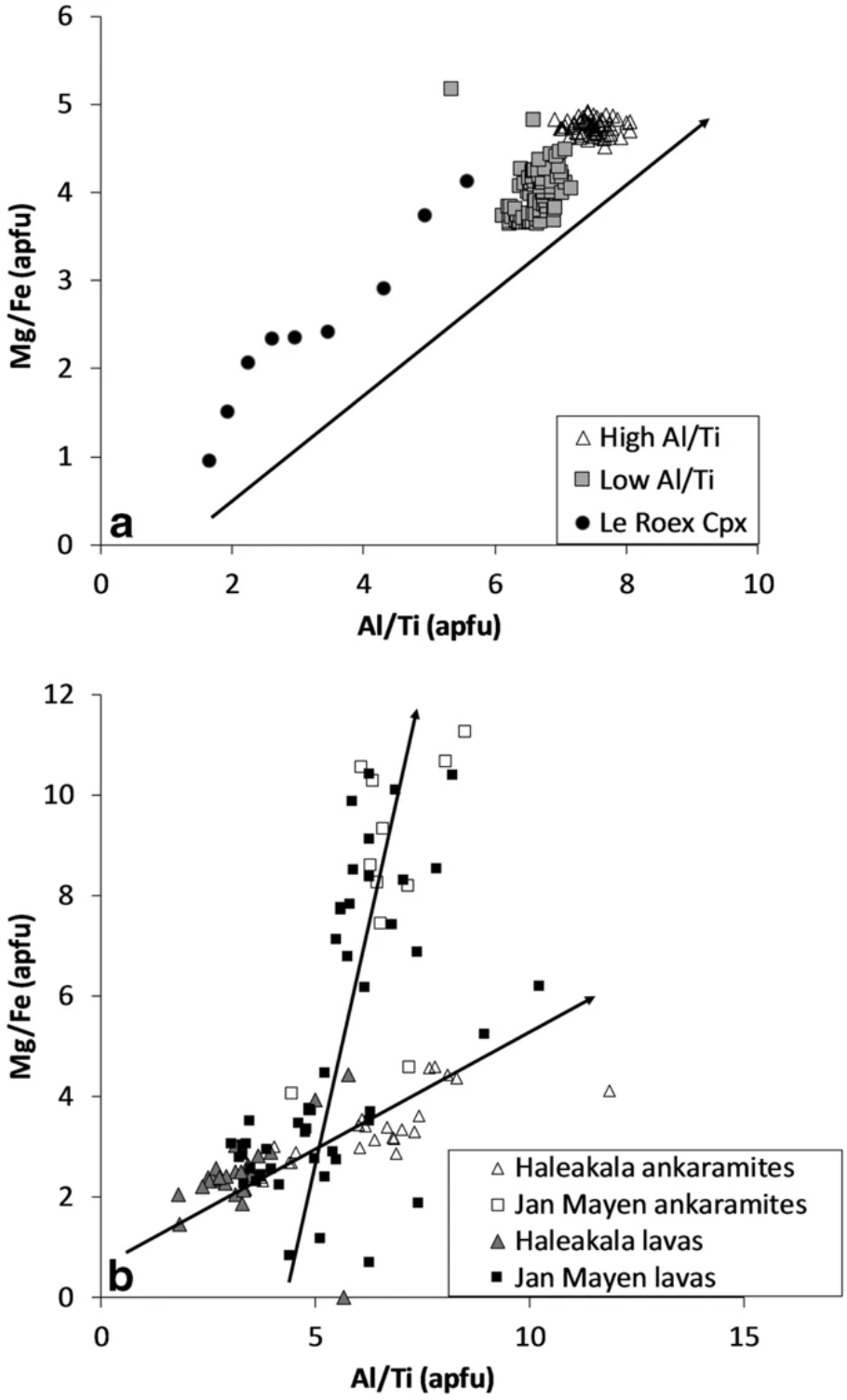

Fig. 10. Plot of Al/Ti versus Mg/Fe for clinopyroxene megacrysts and their associated lavas. **a** Marion Island megacrystic clinopyroxene (this paper) and lava hosted clinopyroxenes (Le Roex et al. 2012), **b** ankaramitic clinopyroxenes from Haleakala (Welsch et al. 2016) and Jan Mayen (Maaløe et al. 1988) and the associated lava-hosted clinopyroxenes

Conclusion

The clinopyroxene megacrysts found in a scoria cone on Marion Island contain olivine inclusions of varying compositions, as well as Ni-rich sulphides and Fe-Ti

oxides. The megacrysts are full of voids despite a generally euhedral appearance, and consist of both low Al-Ti and high Al-Ti clinopyroxene domains. The megacrysts host both primary and secondary olivine crystals. The growth of haematite in olivine indicates that hydrogenation has occurred in some crystals.

The clinopyroxenes are held to have formed in a near-surface magma chamber, where second boiling or the addition of water has created super-saturated conditions for the growth of clinopyroxene. Olivines present in the original magma are incorporated into a non-equilibrium clinopyroxene growing in these super-saturated conditions. As the crystal ascends and the co-existing liquid becomes more volatile-rich, the early formed skeletal clinopyroxene crystal experiences new crystallisation. Multiple decompression episodes would encourage clinopyroxene growth, and it is likely that the clinopyroxenes were never in equilibrium with the co-existing liquid, until finally the crystals are erupted on surface in a fluid-driven scoria eruption.

Acknowledgements

This paper represents the culmination of several years' work, and has relied on the generosity of numerous people for analytical time and interpretation, especially the late Peter Gräser who performed the original EPMA analysis. David Evans, an anonymous reviewer, and associate editor Xisheng Xu are thanked for their comments and revisions on drafts of the paper. Thanks is also given to David Dixon for redrafting the map.

References

Boelhouwers JC, Meiklejohn KI, Holness SD, Hedding DW (2008) Geology, geomorphology and climate change. In: Chown SL, Froneman PW (eds) The Prince Edward islands. Land-sea interactions in a changing ecosystem. African Sunmedia, Johannesburg, pp 65–96

Champness PE (1970) Nucleation and growth of iron oxides in olivines, $(Mg, Fe)_2SiO_4$. Mineral Mag 37(291):790–800

Chevallier L (1986) Tectonics of Marion and Prince Edward volcanoes (Indian Ocean): result of regional control and edifice dynamics. Tectonophysics 124(1):155–175

De Hoog JC, Hattori K, Jung H (2014) Titanium and water-rich metamorphic olivine in high-pressure serpentinites from the Voltri Massif (Ligurian Alps, Italy): evidence for deep subduction of high-field strength and fluid-mobile elements. Contrib Mineral Petrol 167(3):990

Dyar MD, Delaney JS, Sutton SR, Schaefer MW (1998) Fe^{3+} distribution in oxidized olivine: a synchrotron micro-XANES study. Am Mineral 83(12):1361–1365

Hall K, Meiklejohn I, Bumby A (2011) Marion Island volcanism and glaciation. Antarct Sci 23(2):155–163

Hammer J, Jacob S, Welsch B, Hellebrand E, Sinton J (2016) Clinopyroxene in postshield Haleakala ankaramite: 1. Efficacy of thermobarometry. Contrib Mineral Petrol 171(1):1

Hoffman JW, De Beer FC (2012) Characteristics of the Micro-Focus X-ray Tomography Facility (MIXRAD) at Necsa in South Africa. 18th World Conference on Non-Destructive Testing, Durban. http://www.ndt.net/article/wcndt2012/papers/37_wcndtfinal00037.pdf

Hwang SL, Yui TF, Chu HT, Shen P, Iizuka Y, Yang HY, Yang J, Xu Z (2008) Hematite and magnetite precipitates in olivine from the Sulu peridotite: a result of dehydrogenation-oxidation reaction of mantle olivine? Am Mineral 93(7):1051–1060

Ingrin J, Skogby H (2000) Hydrogen in nominally anhydrous upper-mantle minerals: concentration levels and implications. Eur J Mineral 12(3):543–570

Jan C, De Hoog M, Hattori K, Jung H (2014) Titanium-and water-rich metamorphic olivine in high-pressure serpentinites from the Voltri Massif (Ligurian Alps, Italy): evidence for deep subduction of high-field strength and fluid-mobile elements. Contrib Mineral Petrol 167(3):1

Jochum KP, Willbold M, Raczek I, Stoll B, Herwig K (2005) Chemical characterisation of the USGS reference glasses GSA-1G, GSC-1G, GSD-1G, GSE-1G, BCR-2G, BHVO-2G and BIR-1G using EPMA, ID-TIMS, ID-ICP-MS and LA-ICP-MS. Geostand Geoanal Res 29(3):285–302

Khisina NR, Wirth R (2002) Hydrous olivine $(Mg_{1-y}\ Fe^{2+}{}_{y})_{2-x}\ v_x\ SiO_4H_{2x}$– a new DHMS phase of variable composition observed as nanometer-sized precipitations in mantle olivine. Phys Chem Miner 29(2):98–111

Kohlstedt DL, Vander Sande JB (1975) An electron microscopy study of naturally occurring oxidation produced precipitates in iron-bearing olivines. Contrib Mineral Petrol 53(1):13–24

Le Maitre RW, Streckeisen A, Zanettin B, Le Bas MJ, Bonin B, Bateman P (eds) (2005) Igneous rocks: a classification and glossary of terms: recommendations of the International Union of Geological Sciences Subcommission on the Systematics of Igneous Rocks. Cambridge University Press, Cambridge

Le Roex AP, Chevallier L, Verwoerd WJ, Barends R (2012) Petrology and geochemistry of Marion and Prince Edward islands, Southern Ocean: magma chamber processes and source region characteristics. J Volcanol Geotherm Res 223:11–28

Loucks RR (1990) Discrimination of ophiolitic from nonophiolitic ultramafic-mafic allochthons in orogenic belts by the Al/Ti ratio in clinopyroxene. Geology 18(4):346–349

Maaløe S, Pedersen RB, James D (1988) Delayed fractionation of basaltic lavas. Contrib Mineral Petrol 98(4):401–407

McDougall I, Verwoerd W, Chevallier L (2001) K–Ar geochronology of Marion Island, Southern Ocean. Geol Mag 138(01):1–17

Mollo S, Hammer JE (2017) Dynamic crystallization in magmas. In: Heinrich W, Abart R (eds) Mineral reaction kinetics: microstructures, textures, chemical and isotopic signatures. EMU Notes Mineralog, vol 16. European Mineralogical Union and Mineralogical Society of Great Britain and Ireland, London, pp 373–418

Mollo S, Putirka K, Misiti V, Soligo M, Scarlato P (2013) A new test for equilibrium based on clinopyroxene–melt pairs: clues on the solidification temperatures of Etnean alkaline melts at post-eruptive conditions. Chem Geol 352:92–100

Morimoto N (1988) Nomenclature of pyroxenes. Miner Petrol 39(1):55–76

Nimis P, Taylor WR (2000) Single clinopyroxene thermobarometry for garnet peridotites. Part I. calibration and testing of a Cr-in-Cpx barometer and an enstatite-in-Cpx thermometer. Contrib Mineral Petrol 139(5):541–554

Putirka KD (2008) Thermometers and barometers for volcanic systems. In: Putirka KD, Tepley FJ III (eds) Minerals, inclusions and volcanic processes. Rev Mineral Geochem, vol 69. Mineral Soc Am, Chantilly, pp 61–120

Putnis A (2002) Mineral replacement reactions: from macroscopic observations to microscopic mechanisms. Mineral Mag 66(05):689–708

Spear FS (1993) Metamorphic phase equilibria and pressure-temperature-time paths. Miner Soc Am Monograph, Washington DC 799 pp

Stewart ML, Pearce TH (2004) Sieve-textured plagioclase in dacitic magma: interference imaging results. Am Mineral 89(2–3):348–351

Streck MJ (2008) Mineral textures and zoning as evidence for open system processes. In: Putirka KD, Tepley FJ III (eds) Minerals, inclusions and volcanic processes. Rev Mineral Geochem, vol 69. Mineral Soc Am, Chantilly, pp 595–622

Sumner PD, Meiklejohn KI, Boelhouwers JC, Hedding DW (2004) Climate change melts Marion Island's snow and ice: research letter. S Afr J Sci 100(7–8):395–398

Sun SS, McDonough WS (1989) Chemical and isotopic systematics of oceanic basalts: implications for mantle composition and processes. Geol Soc Spec Publ 42(1):313–345

Tomiya A, Takahashi E (2005) Evolution of the magma chamber beneath Usu volcano since 1663: a natural laboratory for observing changing phenocryst compositions and textures. J Petrol 46(12):2395–2426

Vance JA (1965) Zoning in igneous plagioclase: patchy zoning. J Geol 73(4):636–651

Verwoerd WJ (1971) Geology. In: van Zinderen Bakker EM, Winterbottom JM, Dyer RA (eds) Marion and Prince Edward islands: report on the South African biological and geological expedition 1965–1966. AA Balkema, Cape Town, pp 40–62

Verwoerd WJ, Chevallier L, Thomson JW (1990) Oceanic islands on the Antarctic Plate. In: LeMasurier WE, Thompson JW, Baker PE, Kyle PR, Rowley PD, Smellie JL, Verwoerd WJ (eds) Volcanoes of the Antarctic Plate and Southern Oceans, Volume 48. American Geophysical Union, Washington D.C., pp 396–463

Welsch B, Hammer J, Baronnet A, Jacob S, Hellebrand E, Sinton J (2016) Clinopyroxene in postshield Haleakala ankaramite: 2. Texture, compositional zoning and supersaturation in the magma. Contrib Mineral Petrol 171(1):1